Tailoring large pores of porphyrin networks on Ag(111) by metal-organic coordination

Felix Bischoff,[a]§ Yuanqin He,[a, b]§ Knud Seufert,[a] Daphné Stassen,[c] Davide Bonifazi,* [c, d], Johannes V. Barth[a], and Willi Auwärter,*[a, b]

Abstract: The engineering of nano-architectures to achieve tailored properties relevant for macroscopic devices is a key motivation of organo-metallic surface science. To this end, understanding the role of molecular functionalities in structure formation and adatom coordination is of great importance. In this low-temperature scanning tunneling microscopy (STM) study, we elucidate the differences in formation of Cu-mediated metal-organic coordination networks based on two pyridyl- and cyano-bearing free-base porphyrins on Ag(111). Distinct coordination networks evolve *via* different pathways upon codeposition of Cu adatoms. The cyano-terminated module directly forms two-dimensional (2D), porous networks featuring four-fold coordinated Cu nodes. By contrast, the pyridyl species engage in two-fold coordination with Cu and a fully reticulated 2D network featuring a pore size exceeding 3 nm^2 only evolves *via* an intermediate structure based on 1D coordination chains. The STM data and complementary Monte-Carlo simulations reveal that these distinct network architectures originate from spatial constraints at the coordination centers. Furthermore, we demonstrate that Cu adatoms can form two- and four-fold monoatomic coordination nodes with monotopic nitrogen-terminated linkers on the very same metal substrate - a versatility that is not achieved by other 3d transition metal centers but consistent with 3D coordination chemistry. Our study discloses how specific molecular functionalities can be applied to tailor coordination architectures and highlights the potential of Cu as coordination center in such low-dimensional structures on surfaces.

Introduction

Supramolecular coordination chemistry is a vivid field of research as the combination of (metal-) organic ligands and metal centers yield structures and properties that are not achievable by the individual building blocks. Recent examples highlighting the potential of metal-organic compounds include reports alluding on information storage[1] and processing[2], energy storage[3], catalysis[4] and molecular electronics[5]. Considerable efforts were dedicated to adapt design principles from such three-dimensional (3D) supramolecular structures to a two-dimensional (2D) environment represented by surfaces in a controlled ultra-high-vacuum (UHV) setting[6]. Also in this 2D scenario, the functionality of metal-organic coordination networks is represented by the combination of metal nodes, offering e.g., active sites for energy conversion chemistry[7] and the ligands, dictating the pore sizes, the confinement of adsorbates[8] and the (magnetic) coupling between the metals[9]. Specifically, the coordination number and symmetry at the nodes are decisive for the topology of the resulting metal-directed architectures[10]. Despite the manifold

[a]   F. Bischoff, Y. He, Dr. K. Seufert, Prof. W. Auwärter, Prof. J.V. Barth
       Physik Department E20
       Technische Universität München
       85748 Garching (Germany)
       E-Mail: wau@tum.de
       § These authors contributed equally
[b]   Y. He, Prof. W. Auwärter
       Institute for Advanced Study
       Technische Universität München
       85748 Garching (Germany)
[c]   D. Stassen, Prof. D. Bonifazi
       Department of Chemistry and Namur Research College
       University of Namur (Belgium)
[d]   Prof. D. Bonifazi
       School of Chemistry, Cardiff University
       Main Building, Park Place, Cardiff CF10 3AT (United Kingdom)
       Email: bonifazid@cardiff.ac.uk
       Supporting information for this article is given via a link at the end of the document.

reports on surface-anchored metal-organic architectures (see refs

above), strategies to engineer and deliberately tailor assemblies still need to be further developed and refined. For example, extended 2D networks featuring a grid-like structure exhibiting square-shaped pores and mononuclear nodes are rarely reported[11]. In this respect, molecules offering four-fold symmetry might yield advantages compared to the frequently applied ditopic linear linkers. Hereby, tetrapyrroles as porphyrins are ideal candidates, which proved to be stable and versatile building blocks for self-assembled molecular structures on surfaces[12]. The central macrocycle hosting two hydrogens or a metal center adds functionalities to the system, as they can be used as molecular switches[13], can undergo metalation reactions directly on a surface[14] and have potential for heterogeneous catalysis[15] and spintronics[16]. Most importantly, the tetrapyrrole macrocycle can be substituted by a wide variety of terminal moieties, offering vast possibilities to steer intermolecular and metal-organic interactions[11a, 12a-c, 17].

Here, we present a low-temperature scanning tunneling microscopy study comparing the Cu-directed assemblies of two *de-novo* synthesized porphyrins, functionalized with cyano-biphenylene (2H-TPCN) and pyridyl-phenylene substituents (2H-TPyPP), respectively, on Ag(111). Although both molecules feature nitrogen-terminated ligands and assemble into similar organic arrays, they respond markedly differently to the copper atoms. TPCN directly forms 2D metal-organic networks with small pores and four-fold coordination nodes. TPyPP on the other hand follows a hierarchic pathway from 1D metal coordination chains to an open porous 2D metal-organic network with linear two-fold coordinated metal centers. With the help of Monte-Carlo simulation and by comparison of Co- and Cu-directed networks we suggest that the origin of the two- and four-fold coordination motif results from an interplay between the steric hindrance at the coordination center and the inherent coordination properties of Cu.

Results

The 2H-TPCN and 2H-TPyPP modules on Ag(111)

The porphyrins investigated in this study are tetrapyrrolic macrocycles substituted at all four meso-positions either with biphenylene-cyano or with phenylene-pyridyl moieties. Structural models of these two porphyrin derivatives, namely tetra[(4-cyanophenyl)phen-4-yl]porphyrin (2H-TPCN) and tetra[(4-pyridylphenyl)phen-4-yl]porphyrin (2H-TPyPP) are depicted in Figures 1a and d (see also SI).[a] We recently reported on the successful deposition and characterization of 2H-TPCN on Ag(111) and BN/Cu(111)[11c, 18], whereas 2H-TPyPP is addressed in this study for the very first time. Compared to commercially available tetraphenyl- (TPP) or tetrapyridyl-porphyrins (TPyP) featuring only one phenyl or pyridyl unit in each meso-substituent, these novel modules introduce an additional degree of conformational freedom as the terminal ring R_2 can rotate around the C-C single bond between the two phenyl rings R_1 (*cf.* Figures 1a and e). Upon surface confinement, this enhanced molecular flexibility strongly influences the molecular self-assembly and coordination characteristics (*vide infra*). The adsorption of TPP and TPyP species on Ag(111) induces a saddle-shaped macrocycle deformation where the terminal rings are rotated typically 50°- 60° out of the surface plane[13, 19]. A saddle-shape deformation – induced by steric hindrance between the macrocycle and rotated moieties R_1 – is also expected for both 2H-TPCN and 2H-TPyPP. However, as R_1 acts as a spacer geometrically decoupling the terminal rings R_2 from the macrocycle, a rather parallel alignment of R_2 with the Ag(111) surface is anticipated as both, individual benzene and pyridyl rings, adsorb planar on Ag(111)[20]. Figures 1b, c, f and g shows high-resolution STM images of 2H-TPCN and 2H-TPyPP/Ag(111) representing occupied states. Both species present four peripheral lobes associated to the meso-substituents and a donut shape that is assigned to the macrocycle. The latter shows a two-fold symmetry and appears with a depression in the center, as observed previously for free-base TPP on Ag substrates[13]. The elongated meso-substituents of 2H-TPCN are reflected in a larger apparent size of the molecule and an increased intermolecular distance compared to 2H-TPyPP (*vide infra*). Nevertheless, the overall appearance of both species is rather similar, as the cyano group does not contribute considerably to the STM contrast[21]. Based on a comparison of sub-molecular features presented in Figures 1b and f with structural models, a tentative conformation of the meso-substituents' orientation can be inferred. While R_2 looks disk-like indicating a planar adsorption, ring R_1 appears as a narrow bridge connecting the macrocycle and R_2. The asymmetric appearance of R_1 with respect to the axis through the meso-position of the macrocycle (white line in Figures 1b and f) provides an indication for a rotation of R_1. The upper part of the phenyl dominates the image contrast, in full agreement with high-resolution STM data presented in the SI of Ref. 22. Steric hindrance between the rotated R_1 and the pyrroles of the macrocycle leads to its saddle-shape deformation. R_2 appears as a broad protrusion symmetric with respect to the axis connecting opposing legs, in line with the contrast reported for terminal pyridyl groups adsorbed parallel to the Ag(111) surface[22]. We thus conclude that the R_2 rings are aligned approximately parallel to the surface. Note that the larger apparent height of the legs compared to the macrocycle prevails only at small bias voltages

and thus is assigned to an electronic effect (*cf.* Figure S1). As discussed below, the adsorption geometry of the terminal pyridyl rings in TPyPP is decisive for the distinct coordination behavior compared to TPyP, where the pyridyl group is rotated considerably out of the surface plane.
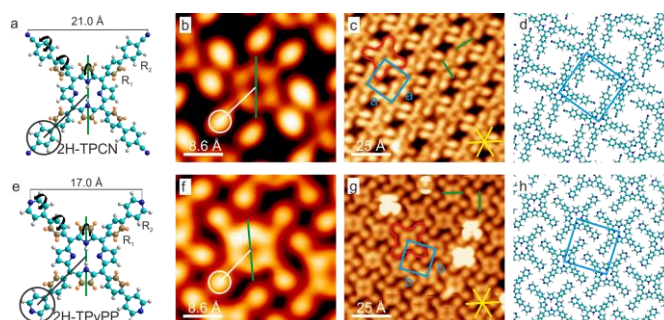

Figure 1. Structural models of the porphyrin derivatives (a and e). The higher parts of rotated molecular moieties are highlighted in orange for better comparison to the zoom-in on single molecules (b and f) within self-assembled, dense-packed islands on Ag(111) (c and g). (d and h) show a sketch of the assembly structure. The green lines highlight the molecular axis through the upward rotated pyrroles. A single molecule is outlined in red in c and g as a guide to the eye and the blue squares indicate the unit cells that include one molecule for both compounds. The substrate dense-packed directions are represented by yellow lines. Scan parameters: (b) $U = -1$ V, $I = 30$ pA; (c) $U = -1$ V, $I = 70$ pA; (f, g) $U = -1$ V, $I = 0.1$ nA.

Self-assembly of 2H-TPCN and 2H-TPyPP on Ag(111)

After room temperature deposition on Ag(111), both modules self-assemble into highly ordered, extended two-dimensional islands (*cf.* Figures 1c and g). The corresponding structural models are shown in Figures 1d and h. Both assemblies feature a square unit cell with internal angles of $(90 \pm 1)°$ (marked in blue in Figures 1c and g) with side length a = (20.4 ± 0.5) Å for 2H-TPCN and side length b = (18.2 ± 0.5) Å for 2H-TPyPP. In addition, a distinct meta-stable structure characterized by a rhombic unit cell can be achieved when depositing 2H-TPCN at high flux (*cf.* Figures S2 and S3). For both porphyrin modules, the molecular axis through the two upward bent pyrroles of the macrocycle (green lines in Figure 1a and e) is either aligned with the $<\overline{1}\overline{1}2>$ or the $<\overline{1}10>$ high symmetry directions of the Ag(111) lattice as indicated by the green lines in Figure 1b and f. While 2H-TPCN mostly aligns along $<\overline{1}\overline{1}2>$ as reported for Co-TPP/Ag(111)[19b], no preference is discernible for 2H-TPyPP. Despite these distinct azimuthal orientations induced by the Ag(111) surface, site-specific interactions do not prevail over lateral intermolecular interactions and the 2H-TPCN and 2H-TPyPP arrays are not commensurate with the underlying Ag(111) lattice, as revealed by bias dependent imaging and dI/dV spectroscopy (*cf.* Figure S1). Both assemblies are stabilized by lateral non-covalent interactions between neighboring nitrogen-phenylene groups.

Formation of metal-organic coordination networks

To investigate the response of the porphyrin species to metal adatoms, Cu was deposited onto sub-monolayer, monomolecular coverages at room temperature. Figure 2 shows the fully reticulated metal-organic coordination networks and the corresponding structural models. For TPCN, a highly regular,

---

[a] The models were created with HyperChem and the molecular dimensions were extracted after geometry optimization of the free molecule within the semi-empirical AM1 framework.

porous network with a rectangular unit cell of size $c = (21.9 \pm 0.5)$ Å and $d = (24.0 \pm 0.5)$ Å evolves featuring domains extending over hundreds of square nanometers with a low defect density (cf. Figure 2a). The long-range order and the symmetry of the network are reflected in the autocorrelation plot and a sharp FFT pattern (Figure 2b). High-resolution images (Figure 2c) reveal details of the network structure, featuring a pore size of approximately 86 Å^2 exposing bare Ag. Clearly, every node – assigned to a Cu adatom – links four TPCN units *via* their carbonitrile termini, resulting in a 1:1 stoichiometric ratio between TPCN and Cu. The projected N-Cu distance is (1.6 ± 0.5) Å, in agreement with the literature reporting on interfacial cyano-Cu coordination.[23] Within the network, the molecules appear slightly compressed compared to the organic phase, i.e., their aspect ratio deviates from the unity, resulting in an "X"-like shape.
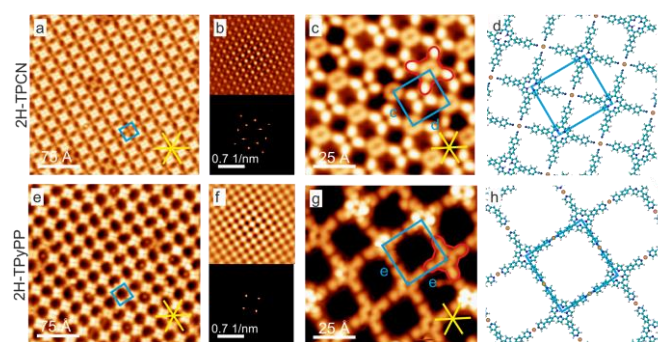

Figure 2. Formation of metal-organic networks upon deposition of Cu atoms. The blue squares indicate the unit cells and one molecular unit is outlined in red as a guide to the eye in (c, g). For TPCN (upper row, (a-d) every coordination node is surrounded by four molecules and the unit cell consists of one molecule and one Cu atom. In contrast, the unit cell of TPyPP/Cu (lower row, (e-h)) consists of one molecule and two Cu atoms. The regularity of the metal-organic networks is reflected in auto-correlation plots (upper image in (b, f)) and sharp spots in FFT images (lower image in (b, f). (d, h) show model sketches of the networks. Differences in the molecular appearance are assigned to the interaction of the macrocycle with Cu adatoms. The yellow stars represent the substrate's dense-packed directions. Scan parameters: (a) $U = 0.7$ V, $I = 50$ pA; (c) $U = 0.2$ V, $I = 0.2$ nA; (e) $U = 0.9$ V, $I = 80$ pA; (g) $U = -0.2$ V, $I = 80$ pA.

This is also reflected in the rectangular unit cell that differs from the square unit cell reported for Gd-coordinated TPCN-networks[18]. The reduced symmetry might be induced by the flexibility of the meso-substituents combined with the favorable hollow site absorption of Cu adatoms on Ag(111)[24]. Indeed, a simple model overlay of the coordination network onto a lattice representing the Ag(111) substrate demonstrates that a highly regular, commensurate (8×80) structure can evolve with Cu adatoms exclusively at hollow sites (see Figure S5 for the details). Apparently the energy gained by formation of the commensurate network – enabled by the specific dimensions of 2H-TPCN – exceeds the energy costs for deforming the molecule. As usual for 3d-transition metals, the coordination center is not visualized in STM[25]. However, an indirect fingerprint of the metal-coordination is observed, as the coordinated terminal groups of TPCN appear higher than those which are non-coordinated (*cf.* Figure S4). For TPCN, fully reticulated metal-organic coordination networks were obtained coexisting with dense-packed organic islands and large Cu clusters on the Ag(111) support under all employed preparation conditions. Thus, the yield for the metal-organic network formation is not optimal at the given preparation temperature and copper flux, however additional architectures based on a simultaneous expression of metal-organic and organic bonding motifs were never observed

for TPCN and Cu[26]. This has been also confirmed by the Monte-Carlo simulations (see below).

Also for TPyPP an extended metal-organic coordination network evolves upon exposure to Cu (cf. Figures 2e and f). It is characterized by a molecule:Cu adatom ratio of 1:2 (Figures 2e and g). All four pyridyl termini of a 2H-TPyPP are connected with the adjacent molecules by pyridyl-Cu-pyridyl coordination motifs, forming a square unit cell with a side length of $e = (28.2 \pm 0.5)$ Å. The projected N-Cu distance amounts to (1.9 ± 0.5) Å in agreement with the literature[25a, 27]. Similar head-on, two-fold Cu-mediated coupling motifs of pyridyl moieties are well-known in surface-confined coordination chemistry[11a, 22b, 25a, 27-28]. Compared to the dense-packed organic arrays, TPyPP modules within the metal-organic network are rotated by 45°. Apparently the energy gain by metal coordination exceeds the energy penalty by deviation from the original adsorption orientation, underlining the weak site-specific molecule-substrate interaction. The network domains extend over hundreds of square nanometers and exhibit long-range regularity (see autocorrelation plot and FFT pattern in Figure 2f). However, high-resolution STM data reveal that the pores vary in size and shape (see Figure 2g). This local disorder is attributed to the flexibility of both the pyridyl-Cu-pyridyl motif – featuring bond angles deviating from 180 ° – and the meso-substituents[22b, 27]. Thus, a variety of pore shapes that deviate from a perfect square can coexist, which classifies this architecture as a 2D short-range disordered crystalline network[29]. The average pore size amounts to 340 Å^2. To our knowledge, such a large area is unprecedented for homo-molecular surface-supported porphyrin-based architectures. Consequently, the Cu-directed TPyPP network might serve as a template to trap and order large adsorbates or even molecular aggregates[30]. To this end, the intrinsic flexibility opens perspectives for hosting and sorting specific molecular guest species, enabling an adaptive behavior of the pores, thus representing a two-dimensional analogue of a "soft porous crystal"[31]. In contrast to the fully reticulated TPCN coordination architecture that evolves directly from the organic islands, the TPyPP coordination follows a hierarchic pathway upon increasing the (local) density of Cu adatoms. After depositing small amounts of Cu adatoms onto a sub-monolayer of 2H-TPyPP/Ag(111), a porous array appears that is characterized by chain-like sub-structures (cf. Figure 3a). A close inspection reveals that it expresses simultaneously metal-organic and organic bonding motifs like those described in Ref. 45. As visualized in the corresponding structural model (Figure 3d), TPyPP tectons are dense-packed in one direction (organic bonding, marked with f) and form a head-on configuration along the other direction (marked with e), which is assigned to a pyridyl-Cu-pyridyl coordination bond, in analogy to the fully reticulated network (cf. Figure 2). The network is thus formed by 1D metal-organic chains that mutually interact via lateral non-covalent interactions between neighboring nitrogen-phenylene groups and follow the dense-packed substrate directions. The structure features a rhomboid unit cell of size $e = (28.0 \pm 0.5)$ Å and $f = (18.2 \pm 0.5)$ Å including an angle of (60 ± 1) ° and a TPyPP to Cu adatom ratio of 1:1.
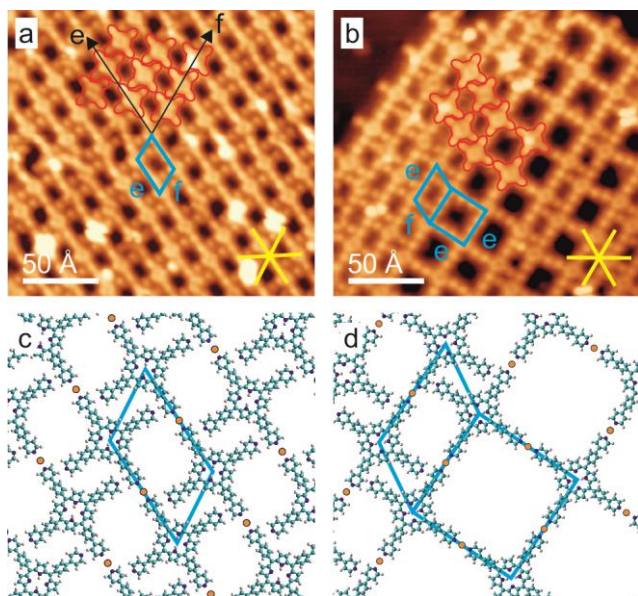
Figure 3. For TPyPP, depending on the (local) Cu density, metal-coordination evolves in one or two directions. (a) The 1D coordination along one specific direction, indicated here by the black arrow labeled with "e", coexists with organic interactions along "f". Coordination will firstly be completed along one direction before starting in another direction as shown in (b). (c and d) show the models. As a guide to the eye, some molecules are outline in red. The yellow stars represent the substrate dense packed directions. Scan parameters (a - c): $U = -0.7$ V, $I = 0.1$ nA.

When the Cu dosage is increased and (locally) exceeds a 1:1 ratio of Cu adatoms to molecules, the organic bonds are transformed to pyridyl-Cu-pyridyl coordination bonds and the structure evolves into a fully reticulated 2D metal-organic network. Figure 3b and the corresponding structural model in Figure 3d show the transition from 1D coordination chains to a 2D coordination network. Both architectures coexist locally and TPyPP can form Cu-coordination bonds to two, three or four adjacent molecules. Clearly, the meso-substituents engaged in coordination bonds appear brighter than their non-coordinated counterparts (*cf.* Figures 3a, c and S4), in line with the results discussed for TPCN.

Monte-Carlo modeling

The experimental results reveal striking differences in the formation of metal-organic coordination networks and the corresponding coordination motifs, despite the similarities of the systems, *i.e.*, mononuclear Cu nodes coordinated to nitrogen of quasi-four-fold symmetric porphyrins on Ag(111). To rationalize the experimental findings, Monte-Carlo modeling was performed as structure formation has been proven to be correctly reproduced in such simple simulations for a variety of functional tectons, including porphyrins[17, 32] and phthalocyanines[33]. For these simulations, both TPyPP and TPCN are represented by a four-fold symmetric cross and metal adatoms are depicted as circles (*cf.* inset in Figure 4a), following a representation previously introduced for similar systems[34]. Within the description of this simplified model, both porphyrin species are identical. To distinguish the two modules, TPyPP is restricted to form one- and two-fold coordination nodes only, as observed in the experiment and TPCN is allowed to engage in one-, two-, three- or four-fold coordination. In Figures 4a-d snapshots of the Monte-Carlo simulations are depicted (see Methods section for details). Naturally, the metal-free dense-packed islands are identical for both species (Figure 4a). After including a small amount of

adatoms, TPyPP shows 1D metal-organic chains (Figure 4b) that evolve into an open-porous 2D coordination network depicted in Figure 4c when adding more metal. Contrary, for TPCN already small amounts of adatoms lead to the formation of a 2D coordination network (Figure 4d). Importantly, the simulations reflect all assemblies observed experimentally and correctly reproduce a key difference between TPyPP and TPCN, namely the fact that 1D metal-organic chains exclusively emerge from TPyPP, Even though they would be allowed for TPCN.

In order to further characterize the system, additional Monte-Carlo simulations were carried out for different interaction energy ratios E_O/E_C (vdW interaction vs. metal-coordination). The results are summarized phase diagrams for TPyPP and TPCN are shown in Figures 4e and f, respectively. To generate these plots, the resulting structures are color-coded in RGB, namely blue (B) for the dense-packed organic network, red (R) for the 1D coordination chains, and green (G) for the 2D metal-organic network (note that the 2D fully reticulated coordination networks are different for the two species (TPyPP in a two-fold fashion and TPCN in a four-fold fashion), despite being both represented in green, as indicated by the insets in Figures 3c and d, respectively). The most prominent difference between the two diagrams is the lack of 1D coordination for TPCN – although allowed – regardless of the ratio of E_O/E_C evidenced by the lack of red in Figure 4f. Apparently, a separation of organic islands and fully reticulated four-fold coordinated arrays is energetically favored over mixed organic/two-fold coordination assemblies. Furthermore, the simulations yield no 1D metal-organic chains for TPCN at any probed temperature (see Methods and Figures S7, S8), thus ruling out any influences of the experimental preparation conditions. The TPyPP structure formation proceeds *via* 1D chains (red, Figure 4d) for all calculated ratios of E_O/E_C, despite the possibility to directly form 2D coordination networks. Therefore, in the case of terminal groups expressing only in a two-fold coordination motif, the observed chaining seems energetically clearly favored even for large relative values of E_C. In the modeling, the only difference between the two species is the permitted coordination geometry at the node, e.g., no effects of the electronic structure are considered. As the simulations qualitatively reproduce the experimentally observed networks, it suggests that the different formation pathways and the resulting network topologies are mainly determined by distinct spatial constraints at the coordination center.
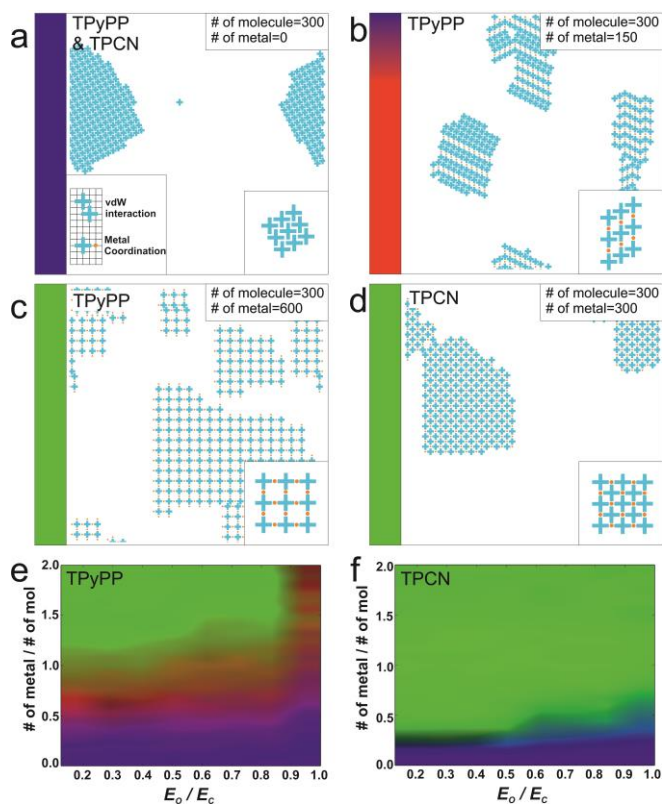
Figure 4. (a –d) Snapshots of the structure formation of porphyrin linkers with metal atoms modeled in Monte-Carlo simulations. (a) 300 molecules and no metal atoms. Without metal atoms both species yield the same assembly. (b) 300 TPyPP and 150 metal atoms. (c) 300 TPyPP and 600 metal atoms and (d) 300 TPCN and 300 metal atoms. The lower-left inset in (a) highlights the two interactions included in the simulations. The bottom-right insets in (a - d) provide a zoom-in on the dominating pattern. (e) and (f) are phase transition diagrams for TPyPP and TPCN respectively, as a function of the relative number of units (# of metal atoms)/(# of molecules) and the ratio of interaction energies E_O/E_C. Due to the finite island sizes, the transition to the coordinated phase (green) proceeds for TPCN already at values of (# of metal atoms)/(# of molecules) below 1 (compare Fig. SI 7).

Discussion

Based on the above findings, the following conclusions can be drawn. Without steric hindrance, Cu adatoms favor a four-fold coordination to the nitrogen termini of porphyrins on Ag(111). In the experiments, this situation is realized for the slender cyano moieties of TPCN. Restricting the nodal symmetry to two-fold by introducing spatial constraints due to (near-)planar pyridyl groups in TPyPP, assemblies featuring 1D coordination chains can be achieved for molecule to adatom ratios ≤ 1:1. Increasing the adatom concentration induces formation of additional pyridyl-Cu-pyridyl links, thus yielding a fully reticulated porous coordination network. Regarding ligands, the observed linear pyridyl-Cu-pyridyl motif was tentatively assigned to steric hindrance by several studies[11a, 22b, 25a, 27]. Only when relaxing these constraints by rotating terminal pyridyl rings out of the surface plane, e.g., by using the TPyP modules, a four-fold coordination to mononuclear centers can be achieved[35] (cf. Figure S6). Such square-planar motifs are well known for pyridyl complexes in 3D coordination chemistry[36], but uncommon in a 2D environment[37]. Their rare occurrence on metallic supports might be attributed to several

aspects: A large adatom - nitrogen distance with respect to the surface induced by the rotation of the pyridyl ring out of the surface plane, weakening the pyridyl –adatom interaction, the nature of the coordinating metal center (*vide infra*) or simply the limited number of studies addressing molecular modules featuring rotated terminal pyridyl moieties. To achieve a four-fold coordination with co-planar adsorbing moieties, a terminal group inducing minor steric constraints is necessary (e.g., cyano group). In this sense, the pyridyl-phenylene substitution of the *de-novo* synthesized 2H-TPyPP providing rotational flexibility to the termini is crucial for the formation of linear pyridyl-Cu-pyridyl binding motifs and for the construction of large-pore Cu-mediated coordination networks. Spatial constraints at the coordination center – tunable by the geometric footprint of the terminal moieties – can be deliberately exploited to control the coordination number and thus the topology of the network architectures. Additionally, the Monte-Carlo simulations show that the spatial constraints of the pyridyls do not only influence the final architectures, but they also induce an energetic preference for the formation of 1D coordination chains and therefore are the origin of the hierarchic assembly protocol in the case of TPyPP.

Regarding the role of the metal center, our experiments reveal that single Cu adatoms – somewhat neglected in on-surface coordination chemistry to date – can link four ligands in a quasi square-planar arrangement. Four-fold mononuclear 3d-metal nodes on metal substrates reminiscent of the square-planar coordination motif have been observed for Mn[38], Fe[35a], Co[21c, 35b] and Ni[9]. Recently, on-surface four-fold coordination was achieved in porphyrin-based metal-organic networks by either applying lanthanide centers[18] that support high coordination numbers[39] or by introducing a boron nitride spacer layer[11c]. To our knowledge, a coordination number of four on surfaces was only reported for Cu dimers[40] in metal-organic networks and for distorted Cu-carboxylate complexes[41]. This study introduces the first coordination network based on a square-planar motif based on monoatomic Cu centers. Accordingly, on Ag(111), Cu adatoms can form coordination bonds to two[22b, 25a, 27, 42], three[43] or four nitrogen atoms. This diversity in on-surface coordination numbers discriminates Cu from other 3d metals as Co, where three-fold coordination reminiscent of the trigonal-planar motif known from 3D coordination chemistry prevails. Even for cross-like TPCN molecule on Ag(111), Co-coordination results in a random metal-organic network in which three- and four-fold nodes coexist[18], thus ruling out a dominating role of the molecular symmetry on the resulting metal-organic architecture. Indeed, a quantitative analysis of coordination geometries of d-block metals in 3D supra-molecular complexes and solid-state structures shows a frequent occurrence of the square-planar and square pyramidal motifs for Cu, which only play a negligible role for Co[44]. Of course, one should be well aware that the metallic surface can drastically influence the coordination behavior, allowing for non-integer oxidation states, coordination spheres unachievable in solution and coordinatively unsaturated centers exposing apical sites to vacuum. This is exemplified by the cyano coordination to Co employing dicarbonitrile-polyphenyl linkers[8a, 45] or Cu using DCA molecules[46]. Furthermore, the metallic surface might mimic an additional ligand[47] and thus reduce the coordination number in the 2D adsorbate systems[8a]. In this picture, the two-fold pyridyl-Cu-pyridyl link translates to a T-shaped coordination sphere of Cu employing three ligands (two pyridyls and the Ag). Indeed such T-shaped motifs are observed for Cu centers in 3D complexes, in contrast to Co preferring tetrahedral or pyramidal geometries[44, 48]. Additionally, TPyP molecules form a four-fold coordination

motif with Fe[35a] but a two-fold coordination with Cu[11a] on Au(111), which fits observations from 3D chemistry where Fe, similar to Co, strongly prefers coordination to four or more partners. Thus, in addition to the important steric constraints induced by the pyridyl rings adsorbed approximately parallel to the surface as discussed above, the naturally preferred coordination geometries of Cu itself might contribute to the stabilization of the linear pyridyl-Cu-pyridyl motif prevalent on coinage metal surfaces and at the same time support the four-fold coordination in the case of TPCN.

Conclusion

Summarizing, by exploiting the preferred coordination geometries of copper in combination with a deliberate porphyrin functionalization, we were able to design extended, 2D, grid-like metal-organic coordination networks on Ag(111). Both TPCN and TPyPP thus offer a basis for the fabrication of bimetallic[18] and mixed valence[11a] open porous networks *via* orthogonal insertion of metals[18]. Additionally for TPyPP, the large pore size and the flexibility of the pyridyl-Cu-pyridyl links result in 2D structure reminiscent of a soft-porous-crystal, providing opportunities to act as a template for the selective adsorption of molecular guests or nanostructures[12g].

To rationalize the formation of distinct Cu-mediated structures from TPCN and TPyPP, we performed Monte-Carlo simulations and related the experimental findings to reports on Co-mediated coordination networks and metal-organic complexes in solution chemistry. This comparison reveals that the choice of the coordinating metal is decisive for the emerging coordination motif, *e.g.*, replacing Co by Cu in TPCN coordination assemblies results in a highly regular network as compared to a random structure. Here, coordination geometries in 3D metal-organic complexes can provide some clues for an appropriate selection of suitable metal for a targeted motif. E.g., Co preferentially binds in a tetrahedral fashion and therefore is no promising candidate for the formation of linear, two-fold coordination motifs on surfaces. Cu on the other hand is identified by our study as versatile center supporting different coordination numbers and geometries. Using TPCN, we achieved the first surface-based coordination network based on a four-fold motif and mononuclear Cu center. Additionally, our study indicates that the ligand properties (*e.g.*, rotated *vs.* planar pyridyls *vs.* cyano moieties) must fit the targeted nodal geometry and thus can be used to tailor the resulting network structure and their formation pathway *via* spatial constraints. Furthermore, we demonstrated the benefits of basic Monte-Carlo simulations in selecting suitable molecular modules for metal-organic architectures prior to the actual experiment. Consequently, our study introduces prospects for the programmed design and selection of molecular and monoatomic building blocks for surface-confined supramolecular networks and thus contributes to a controlled engineering of metal-organic organic architectures.

Experimental Section

Experimental procedures

All experiments were performed in a custom designed ultra-high vacuum chamber housing a commercial STM (www.createc.de) operated at 5 K.

The base pressure during the experiments was below 3×10^{-10} mbar. Repeated cycles of Ar+ sputtering and annealing to 725 K were used to prepare the Ag(111) single crystal. 2H-TPyPP and 2H-TPCN molecules were dosed from a thoroughly degassed quartz crucible held at 760 K. During deposition the sample was kept at room temperature. Cu was evaporated from a home-built, water-cooled cell by resistively heating a W filament supporting a Cu wire of high purity (99.9999%). All STM images were recorded in constant current mode using an electrochemically etched tungsten tip prepared by sputtering and controlled dipping into the Ag(111) substrate. In the figure captions voltage *U* refers to the bias voltage applied to the sample. The WsXM program (www.nanotec.es) was used to process the STM raw data.

Monte-Carlo simulation

A square lattice with 100 x 100 points is used as substrate due to the shape of the molecules. Both TPyPP and TPCN are represented by a cross that occupies five lattice sites, a metal atom fills one lattice site (*cf.* inset in Figure 4a). Only two intermolecular interactions are considered and are limited to be short-ranged and directional, *i.e.*, they reach one lattice site along the direction of the molecular substituents. The first one is vdW interaction E_O occurring when two molecules align in a dense-packed fashion (see top right inset in Figure 4a). The second one describes metal-coordination with interaction energy E_C between molecules and metal adatoms. It can only be formed when the metal atom is placed on a lattice site right at the end of a molecular substituent. For TPyPP, the metal atom is restricted to form one- or two-fold coordination to mimic steric hindrance. Thus, a metal atom can express coordination bonds with a maximum of two TPyPPs, which have to be on opposite sides of the metal atom. On contrary, a metal atom can coordinate up to four TPCN. The molecule-substrate interaction is neglected, which is a reasonable approximation, as the experimental observations reveal no relevant site-specific molecule-substrate bonding. In the simulations, E_C is kept constant at a value of 40 (expressed in kT units of energy) while E_O is varied from 5 to 40. These values are selected by considering both theoretical values of the bonding energies and experimental results. According to the literature, the bonding energy of a Cu-N coordination bond varies from 0.5 to 2 eV for 3D systems[49] and the energy of non-covalent bonds, here T-type[50] or PARI interactions[51], range from 40 to 80 meV. As described in the experimental section, molecules are deposited at room temperature, which means the formation temperature of the self-assembly should be less than or equal to this value. On the other hand, stable dense-packed islands of TPP have been observed at room temperature[52], indicating that at this temperature the bonding energies already exceed the thermal energy. Therefore it is reasonable to choose a temperature range from 200 to 250 K in the simulation. Using these values to express the bonding energies in kT units, we get $E_C = 40$ and $E_O = 5$ (*vide supra*). The number of molecules is kept constant at 300. The simulation procedure follows the protocol described in reference[53].

References

[1] G. A. Craig and M. Murrie, *Chem. Soc. Rev.* **2015**, *44*, 2135-2147.

[2] S. Gao, *Molecular Nanomagnets and Related Phenomena*, Springer Berlin Heidelberg, Berlin, Heidelberg, **2015**, p. 164.

[3] a) L. Lux, K. Williams and S. Ma, *CrystEngComm* **2015**, *17*, 10-22; b) F.-S. Ke, Y.-S. Wu and H. Deng, *J. Solid State Chem.* **2015**, *223*, 109-121.

[4] K. Leus, Y.-Y. Liu and P. V. D. Voort, *Catal. Rev.* **2014**, *56*, 1-56.

[5] M. Ruben, J. Rojo, F. J. Romero-Salguero, L. H. Uppadine and J.-M. Lehn, *Angew. Chem. Int. Ed.* **2004**, *43*, 3644-3662.

[6] a) J. V. Barth, G. Costantini and K. Kern, *Nature* **2005**, *437*, 671–679; b) L. Bartels, *Nat. Chem.* **2010**, *2*, 87–95; c) N. Lin, S. Stepanow, M. Ruben and J. V. Barth in *Surface-confined supramolecular coordination chemistry*, *Vol.* Springer, **2008**, pp. 1–44.

[7] a) R. Gutzler, S. Stepanow, D. Grumelli, M. Lingenfelder and K. Kern, *Acc. Chem. Res.* **2015**, *48*, 2132-2139; b) D. Grumelli, B. Wurster, S. Stepanow and K. Kern, *Nat. Commun.* **2013**, *4*, 2904.

[8] a) U. Schlickum, R. Decker, F. Klappenberger, G. Zoppellaro, S. Klyatskaya, M. Ruben, I. Silanes, A. Arnau, K. Kern, H. Brune and J. V. Barth, *Nano Lett.* **2007**, *7*, 3813-3817; b) R. Decker, U. Schlickum, F. Klappenberger, G. Zoppellaro, S. Klyatskaya, M. Ruben, J. V. Barth and H. Brune, *Appl. Phys. Lett.* **2008**, *93*, 243102; c) D. Kühne, F. Klappenberger, W. Krenner, S. Klyatskaya, M. Ruben and J. V. Barth, *Proc. Natl. Acad. Sci. USA* **2010**, *107*, 21332-21336; d) S. Nowakowska, A. Wäckerlin, S. Kawai, T. Ivas, J. Nowakowski, S. Fatayer, C. Wäckerlin, T. Nijs, E. Meyer, J. Björk, M. Stöhr, L. H. Gade and T. A. Jung, *Nat. Commun.* **2015**, *6*, 6071; e) R. Zhang, G. Lyu, C. Chen, T. Lin, J. Liu, P. N. Liu and N. Lin, *ACS Nano* **2015**, *9*, 8547-8553.

[9] N. Abdurakhmanova, T.-C. Tseng, A. Langner, C. S. Kley, V. Sessi, S. Stepanow and K. Kern, *Phys. Rev. Lett.* **2013**, *110*, 027202.

[10] G. E. Pacchioni, M. Pivetta and H. Brune, *J. Phys. Chem. C* **2015**, *119*, 25442-25448.

[11] a) Y. Li, J. Xiao, T. E. Shubina, M. Chen, Z. Shi, M. Schmid, H.-P. Steinrück, J. M. Gottfried and N. Lin, *J. Am. Chem. Soc.* **2012**, *134*, 6401-6408; b) S. Stepanow, M. Lingenfelder, A. Dmitriev, H. Spillmann, E. Delvigne, N. Lin, X. Deng, C. Cai, J. V. Barth and K. Kern, *Nat. Mater.* **2004**, *3*, 229-233; c) J. I. Urgel, M. Schwarz, M. Garnica, D. Stassen, D. Bonifazi, D. Ecija, J. V. Barth and W. Auwärter, *J. Am. Chem. Soc.* **2015**, *137*, 2420-2423.

[12] a) W. Auwärter, D. Écija, F. Klappenberger and J. V. Barth, *Nat. Chem.* **2015**, *7*, 105-120; b) J. M. Gottfried, *Surf. Sci. Rep.* **2015**, *70*, 259-379; c) S. Mohnani and D. Bonifazi, *Coord. Chem. Rev.* **2010**, *254*, 2342-2362; d) L.-A. Fendt, M. Stöhr, N. Wintjes, M. Enache, T. A. Jung and F. Diederich, *Chem. Eur. J.* **2009**, *15*, 11139–11150; e) N. Wintjes, J. Lobo-Checa, J. Hornung, T. Samuely, F. Diederich and T. A. Jung, *J. Am. Chem. Soc.* **2010**, *132*, 7306–7311; f) C. Iacovita, P. Fesser, S. Vijayaraghavan, M. Enache, M. Stöhr, F. Diederich and T. A. Jung, *Chem. Eur. J.* **2012**, *18*, 14610–14613; g) F. Sedona, M. Di Marino, M. Sambi, T. Carofiglio, E. Lubian, M. Casarin and E. Tondello, *ACS Nano* **2010**, *4*, 5147–5154.

[13] W. Auwärter, K. Seufert, F. Bischoff, D. Ecija, S. Vijayaraghavan, S. Joshi, F. Klappenberger, N. Samudrala and J. V. Barth, *Nat. Nanotechnol.* **2011**, *7*, 41–46.

[14] a) H. Marbach, *Acc. Chem. Res.* **2015**, *48*, 2649-2658; b) J. I. Urgel, D. Ecija, W. Auwärter, D. Stassen, D. Bonifazi and J. V. Barth, *Angew. Chem. Int. Ed.* **2015**, *54*, 6163-6167; c) K. Diller, A. C. Papageorgiou, F. Klappenberger, F. Allegretti, J. V. Barth and W. Auwärter, *Chem. Soc. Rev.* **2016**, 45, 1629-1656

[15] B. Hulsken, R. Van Hameren, J. W. Gerritsen, T. Khoury, P. Thordarson, M. J. Crossley, A. E. Rowan, R. J. M. Nolte, J. A. A. W. Elemans and S. Speller, *Nat. Nanotechnol.* **2007**, *2*, 285-289.

[16] C. Wäckerlin, K. Tarafder, J. Girovsky, J. Nowakowski, T. Hählen, A. Shchyrba, D. Siewert, A. Kleibert, F. Nolting, P. M. Oppeneer, T. A. Jung and N. Ballav, *Angew. Chem. Int. Ed.* **2013**, *52*, 4568-4571.

[17] T. Lin, X. S. Shang, J. Adisoejoso, P. N. Liu and N. Lin, *J. Am. Chem. Soc.* **2013**, *135*, 3576-3582.

[18] J. I. Urgel, D. Ecija, W. Auwärter, D. Stassen, D. Bonifazi and J. V. Barth, *Angew. Chem. Int. Ed.* **2015**, *54*, 6163-6167.

[19] a) W. Auwärter, A. Weber-Bargioni, A. Riemann, A. Schiffrin, O. Gröning, R. Fasel and J. V. Barth, *J. Chem. Phys.* **2006**, *124*, 194708; b) W. Auwärter, K. Seufert, F. Klappenberger, J. Reichert, A. Weber-Bargioni, A. Verdini, D. Cvetko, M. Dell' Angela, L. Floreano, A. Cossaro and others, *Phys. Rev. B* **2010**, *81*, 245403.

[20] P. Avouris and J. E. Demuth, *J. Chem. Phys.* **1981**, *75*, 4783-4794.

[21] a) S. Gottardi, K. Müller, J. C. Moreno-López, H. Yildirim, U. Meinhardt, M. Kivala, A. Kara and M. Stöhr, *Adv. Mater. Interfaces* **2014**, *1*; b) M. Marschall, J. Reichert, K. Seufert, W. Auwärter, F. Klappenberger, A. Weber-Bargioni, S. Klyatskaya, G. Zoppellaro, A. Nefedov, T. Strunskus, C. Wöll, M. Ruben and J.

V. Barth, *ChemPhysChem* **2010**, *11*, 1446-1451; c) M. Marschall, J. Reichert, A. Weber-Bargioni, K. Seufert, W. Auwärter, S. Klyatskaya, G. Zoppellaro, M. Ruben and J. V. Barth, *Nat. Chem.* **2010**, *2*, 131–137.

[22] a) D. Heim, D. Ecija, K. Seufert, W. Auwärter, C. Aurisicchio, C. Fabbro, D. Bonifazi and J. V. Barth, *J. Am. Chem. Soc.* **2010**, *132*, 6783–6790; b) D. Heim, K. Seufert, W. Auwärter, C. Aurisicchio, C. Fabbro, D. Bonifazi and J. V. Barth, *Nano Lett.* **2010**, *10*, 122-128; c) D. Ecija, M. Marschall, J. Reichert, A. Kasperski, D. Nieckarz, P. Szabelski, W. Auwärter and J. V. Barth, *Surf. Sci.* **2016**, *643*, 91-97; d) T. Kaposi *et al.*, *in preparation*

[23] M. Pivetta, G. E. Pacchioni, E. Fernandes and H. Brune, *J. Chem. Phys.* **2015**, *142*, 101928.

[24] a) M. Mińkowski and M. A. Załuska-Kotur, *Surf. Sci.* **2015**, *642*, 22-32; b) S. S. Hayat, M. Alcántara Ortigoza, M. A. Choudhry and T. S. Rahman, *Phys. Rev. B* **2010**, *82*, 085405.

[25] a) S. L. Tait, A. Langner, N. Lin, S. Stepanow, C. Rajadurai, M. Ruben and K. Kern, *J. Phys. Chem. C* **2007**, *111*, 10982-10987; b) N. Henningsen, R. Rurali, C. Limbach, R. Drost, J. I. Pascual and K. J. Franke, *J. Phys. Chem. Lett.* **2011**, *2*, 55-61.

[26] S. Vijayaraghavan, D. Ecija, W. Auwärter, S. Joshi, K. Seufert, M. Drach, D. Nieckarz, P. Szabelski, C. Aurisicchio, D. Bonifazi and J. V. Barth, *Chem. Eur. J.* **2013**, *19*, 14143-14150.

[27] D. Heim, D. Écija, K. Seufert, W. Auwärter, C. Aurisicchio, C. Fabbro, D. Bonifazi and J. V. Barth, *J. Am. Chem. Soc.* **2010**, *132*, 6783-6790.

[28] T. R. Umbach, M. Bernien, C. F. Hermanns, L. L. Sun, H. Mohrmann, K. E. Hermann, A. Krüger, N. Krane, Z. Yang, F. Nickel, Y.-M. Chang, K. J. Franke, J. I. Pascual and W. Kuch, *Phys. Rev. B* **2014**, *89*, 235409.

[29] a) D. Ecija, S. Vijayaraghavan, W. Auwärter, S. Joshi, K. Seufert, C. Aurisicchio, D. Bonifazi and J. V. Barth, *ACS Nano* **2012**, *6*, 4258-4265; b) H. Spillmann, A. Kiebele, M. Stöhr, T. A. Jung, D. Bonifazi, F. Cheng and F. Diederich, *Adv. Mater.* **2006**, *18*, 275-279.

[30] C.-A. Palma, J. Björk, F. Klappenberger, E. Arras, D. Kühne, S. Stafström and J. V. Barth, *Nat. Commun.* **2015**, *6*, 6210.

[31] a) S. Horike, S. Shimomura and S. Kitagawa, *Nat. Chem.* **2009**, *1*, 695-704; b) T. Sirtl, S. Schlögl, A. Rastgoo-Lahrood, J. Jelic, S. Neogi, M. Schmittel, W. M. Heckl, K. Reuter and M. Lackinger, *J. Am. Chem. Soc.* **2013**, *135*, 691-695.

[32] a) T. Lin, X. S. Shang, P. N. Liu and N. Lin, *J. Phys. Chem. C* **2013**, *117*, 23027-23033; b) T. Lin, Q. Wu, J. Liu, Z. Shi, P. N. Liu and N. Lin, *J. Chem. Phys.* **2015**, *142*, 101909.

[33] A. Kasperski and P. Szabelski, *Adsorption* **2012**, *19*, 283-289.

[34] A. Kasperski, D. Nieckarz and P. Szabelski, *Surf. Sci.* **2015**, *641*, 269-277.

[35] a) T. Lin, G. Kuang, W. Wang and N. Lin, *ACS Nano* **2014**, *8*, 8310-8316; b) M. E. Garah, A. Ciesielski, N. Marets, V. Bulach, M. W. Hosseini and P. Samorì, *Chem. Commun.* **2014**, *50*, 12250-12253.

[36] a) G. J. Long and P. J. Clarke, *Inorg. Chem.* **1978**, *17*, 1394-1401; b) Y. Agnus, M. Labarelle, R. Louis and B. Metz, *Acta Crystallographica Section C Crystal Structure Communications* **1994**, *50*, 536-538; c) D. J. Hamm, J. Bordner and A. F. Schreiner, *Inorg. Chim. Acta* **1973**, *7*, 637-641.

[37] A. Dmitriev, H. Spillmann, N. Lin, J. V. Barth and K. Kern, *Angew. Chem.* **2003**, *115*, 2774-2777.

[38] a) T.-C. Tseng, C. Lin, X. Shi, S. L. Tait, X. Liu, U. Starke, N. Lin, R. Zhang, C. Minot, M. A. Van Hove, J. I. Cerdá and K. Kern, *Phys. Rev. B* **2009**, *80*, 155458; b) N. Abdurakhmanova, A. Floris, T.-C. Tseng, A. Comisso, S. Stepanow, A. De Vita and K. Kern, *Nat. Commun.* **2012**, *3*, 940.

[39] G. Lyu, Q. Zhang, J. I. Urgel, G. Kuang, W. Auwärter, D. Ecija, J. V. Barth and N. Lin, *Chem. Commun.* **2015**.

[40] A. Breitruck, H. E. Hoster, C. Meier, U. Ziener and R. J. Behm, *Surf. Sci.* **2007**, *601*, 4200-4205.

[41] N. Lin, A. Dmitriev, J. Weckesser, J. V. Barth and K. Kern, *Angew. Chem. Int. Ed.* **2002**, *41*, 4779-4783.

[42] A. Langner, S. L. Tait, N. Lin, R. Chandrasekar, M. Ruben and K. Kern, *Angew. Chem. Int. Ed.* **2008**, *47*, 8835-8838.

[43] S. L. Tait, A. Langner, N. Lin, R. Chandrasekar, O. Fuhr, M. Ruben and K. Kern, *ChemPhysChem* **2008**, *9*, 2495-2499.

[44] D. Venkataraman, Y. Du, S. R. Wilson, K. A. Hirsch, P. Zhang and J. S. Moore, *J. Chem. Educ.* **1997**, *74*, 915.

[45] M. Etzkorn et al., *In preparation*.

[46] G. Pawin, K. L. Wong, D. Kim, D. Sun, L. Bartels, S. Hong, T. S. Rahman, R. Carp and M. Marsella, *Angew. Chem.* **2008**, *120*, 8570-8573.

[47] K. Flechtner, A. Kretschmann, H.-P. Steinrück and J. M. Gottfried, *J. Am. Chem. Soc.* **2007**, *129*, 12110-12111.

[48] W. Hieringer, K. Flechtner, A. Kretschmann, K. Seufert, W. Auwärter, J. V. Barth, A. Görling, H.-P. Steinrück and J. M. Gottfried, *J. Am. Chem. Soc.* **2011**, *133*, 6206-6222.

[49] a) C. F. Faul and M. Antonietti, *Adv. Mater.* **2003**, *15*, 673–683; b) J. V. Barth, *Annu. Rev. Phys. Chem.* **2007**, *58*, 375–407; c) D.-Y. Wu, B. Ren, Y.-X. Jiang, X. Xu and Z.-Q. Tian, *J. Phys. Chem. A* **2002**, *106*, 9042–9052.

[50] a) O. Bludský, M. Rubeš, P. Soldán and P. Nachtigall, *J. Chem. Phys.* **2008**, *128*, 114102; b) S. Tsuzuki, K. Honda, T. Uchimaru, M. Mikami and K. Tanabe, *J. Am. Chem. Soc.* **2002**, *124*, 104–112.

[51] E. Arras, A. P. Seitsonen, F. Klappenberger and J. V. Barth, *Phys. Chem. Chem. Phys.* **2012**, *14*, 15995.

[52] a) L. Scudiero, D. E. Barlow and K. W. Hipps, *J. Phys. Chem. B* **2000**, *104*, 11899–11905; b) K. Comanici, F. Buchner, K. Flechtner, T. Lukasczyk, J. M. Gottfried, H.-P. Steinrück and H. Marbach, *Langmuir* **2008**, *24*, 1897–1901.

[53] D. Nieckarz and P. Szabelski, *J. Phys. Chem. C* **2013**, *117*, 11229-11241.
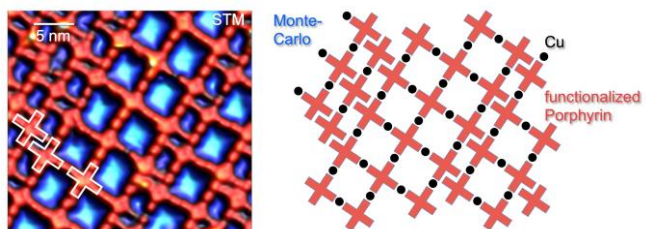
TOC graphic

Porous grid-like porphyrin networks: A scanning tunneling microsopy study of two similar, but distinctly functionalized, porphyrin tectons combined with Monte Carlo modeling reveals how steric hindrance at Cu coordination nodes guides the assembly of networks with unprecedented morphology and pore size.